Apollo 15 regolith breccia provides first natural evidence for olivine incongruent melting – REVISION 1

Niccolò Satta[1, 2, *], Masaaki Miyahara[3], Shin Ozawa[4], Hauke Marquardt[2], Masahiko Nishijima[5], Tomoko Arai[6] and Eiji Ohtani[4]

[1]Bayerisches Geoinstitut, Universität Bayreuth, Bayreuth 95440, Germany

[2]Department of Earth Sciences, University of Oxford, Oxford OX1 3AN, United Kingdom

[3]Department of Earth and Planetary Systems Science, Graduate School of Science, Hiroshima University, Higashi-Hiroshima 739-8526, Japan

[4]Department of Earth Science, Graduate School of Science, Tohoku University, Sendai 980-8578, Japan

[5]Laboratory for Protein Crystallography and Laboratory for Electron Structural Biology Institute for Protein Research, Osaka University, Suita-shi Osaka 565-0871, Japan

[6]Planetary Exploration Research Center, Chiba Institute of Technology, Chiba 275-0016, Japan

Corresponding author: Niccolò Satta (niccolo.satta@earth.ox.ac.uk)

Keywords: ferropericlase, olivine incongruent melting, Apollo 15

Abstract

The Apollo 15 mission has returned various samples of regolith breccias to the Earth – typical lunar rocks lithified by impact events on the Moon's surface. Here we report our observations on shock features recorded in a section of the Apollo Sample 15299. We observe the presence of ferropericlase crystals confined in a shock melt pocket and conclude that their formation is related to a shock-induced incongruent melting of olivine. While predicted by experiments, this phenomenon has never been observed in a natural sample. The incongruent melting of olivine provides an important signature of melting under high-pressure conditions, and allows for estimating the pressure (*P*)-temperature (*T*) experienced by the studied sample during the impact event. We infer that the fracture porosity that likely characterized the studied sample prior to the

shock event critically affects the *P-T* path during the shock compression, and allowed the studied sample to be subjected to elevated temperature during relatively low shock pressures.

Introduction

Collisional processes are integral to the formation and evolution of rocky planets in the Solar System and likely beyond (e.g., Morbidelli et al. 2012). Impacts can result in the propagation of shock waves triggering a temporary, but rapid increase in pressure (*P*) and temperature (*T*). Such events can leave a record in terms of shock features including shock-melt pockets and veins in both impactor and impacted bodies (Langenhorst and Hornemann 2005), as for example shown in recovered meteorites (Gillet and El Goresy 2013). Shock-related phase reactions and transformations can be used to constrain dynamic event(s) in terms of *P-T* conditions, hence can be used to define the shock event history of the studied sample (Gillet et al. 2007).

The presence of numerous impact craters on the Moon's surface provides evidence for a long history of dynamic events, and shock-induced phase transformations are relatively common in lunar meteorites (e.g., Kayama et al., 2018; Miyahara et al., 2013; Ohtani et al., 2011). However, the description of high-pressure polymorphs in lunar rocks is limited to the single case of SiO_2 stishovite (Kaneko et al. 2015).

Olivine [α-$(Mg,Fe)_2SiO_4$] is the most common rock-forming mineral of Earth's upper mantle (Frost 2008). Along the mantle geotherm, olivine transforms into β-$(Mg,Fe)_2SiO_4$ wadsleyite at ~410 kilometres depth. Wadsleyite transforms into γ-$(Mg,Fe)_2SiO_4$ ringwoodite at greater depths (~520 km) (Frost 2008), that eventually dissociates into an assemblage of $(Mg,Fe)O$ ferropericlase + $(Mg,Fe)SiO_3$ bridgmanite in the lower mantle (660-670 km depth) (Ito and Takahashi 1989). Shock-induced phase transitions of olivine into wadsleyite and/or ringwoodite, as well as the

DOI: https://doi.org/10.2138/am-2022-8121. http://www.minsocam.org/

dissociation into (Mg,Fe)O ferropericlase + (Mg,Fe)SiO_3 bridgmanite, have been previously reported in shocked meteorites, and used to constrain the *P*-*T*-conditions of the impact event that lead to their formation (Miyahara et al. 2011, 2016; Tschauner et al. 2014; Bindi et al. 2020). While this phase transition sequence is expected along a typical geotherm, olivine can melt incongruently at pressures as low as 10-15 GPa when subjected to high temperatures (> ~2200 °C), leading to the formation of ferropericlase (Mg,Fe)O + liquid (Presnall and Walter 1993; Ohtani et al. 1998). Here we investigated a shock-melt pocket contained in a lunar rock polished section (Apollo Section 15299,247) combining Raman spectroscopy, Field-Emission Gun Scanning Electron microscopy (FEG-SEM) and Transmission Electron Microscopy (TEM). Our results provide the first observation of ferropericlase with the estimated composition of $(Mg_{0.05-0.68}Fe_{0.95-0.32})O$ in a lunar rock. By combining our observation with previous findings, we conclude that the lunar ferropericlase has been formed by incongruent melting of olivine induced by a dynamic event. We speculate that the fracture porosity characteristic of lunar rocks translates into elevated temperature even at relatively low shock pressures.

Materials and Methods

The Apollo Section 15299,247 (hereafter S247) was obtained from a lunar rock collected during the Apollo 15 mission, namely the Apollo Sample 15299, sampled in the vicinity of station 6 (Swann et al. 1972). An extensive description of modal petrology as well as chemistry of the main mineralogical constituents of this and other Apollo 15 samples can be found in Simon et al. (1986). Detailed textural observations were carried out using a FEG-SEM system (JEOL JSM-7000F) operated with an accelerating voltage of 15 kV, where chemical analysis were performed using the integrated Energy Dispersive Spectrometry (EDS) system. Minerals were identified using micro-

Raman spectroscopy (JASCO NRS-4100TOR). No high-pressure polymorphs such as wadsleyite, ringwoodite, majorite, akimotoiite, and bridgmanite were observed. We employed a gallium (Ga^+) ion beam accelerated with 30 kV in a Focused Ion Beam (FIB) system (FEI Quanta 200 3D) to extract and prepare a ~100 nm thin slice from S247. The polished slice was placed on a molybdenum grid for TEM observations using a manipulator (Omni Probe) implemented in the FIB system. High-angle annular dark field (HAADF) and bright-field TEM images, as well as selected area electron diffraction (SAED) patterns were acquired using a field emission gun TEM JEOL 2100F microscope operating at 200 kV. The camera length and wavelength of the electron beam for SAED analyses were calibrated using a gold particle. Chemical analyses were performed running the TEM in scanning mode and using the EDS detector implemented in the JEOL JEM-2100F. Resulting compositions were calibrated following experimentally determined *k* factors (San Carlos olivine, ferropericlase, and pyrope).

Results

The S247 section is essentially composed of a basalt clast that mainly consists of equigranular low-Ca pyroxene and anorthitic plagioclase phenocrystals (~500 μm across). Olivine is also present but in minor quantities, while chromite and ilmenite appear only as accessory components. This petrographic description is consistent with previous descriptions on a basalt clast included in a different section extracted from the same Apollo Sample 15299, in which finding of shocked SiO_2 stishovite was documented (Kaneko et al. 2015). Similarly to the section studied by Kaneko et al. (2015), S247 shows only minor shock features that can be summarized as a relatively small network of shock-melt veins up to 50 μm in width (e.g., Figure 1a), and shock-melt pockets (Figure 1b).

DOI: https://doi.org/10.2138/am-2022-8121. http://www.minsocam.org/

We focused our investigation on a shock-melt pocket entirely confined in a fractured olivine grain (Figure 1b), which we refer to as pocket in the following for simplicity. SEM observation indicates the coexistence of at least two different phases in the pocket matrix distinguishable as relatively large darkish grains (up to 1 μm diameter grains), and as bright spherules (~50 nm in diameter). In addition, the bright spherules appear to be heterogeneously distributed, becoming more abundant from the inner towards the outer region (from left to right in Figure 1c). Contrarily, the largest darkish grains appear to be mostly localized in the inner region of the pocket.

The bulk compositions of both inner and outer regions were constrained by SEM-EDS analyses rastering the electron beam over the region at target. A total number (*n*) of 5 and 6 analyses were conducted on the inner and outer region, respectively. The resulting bulk compositions were then averaged, with uncertainties estimated as 1 standard deviation between the measurements. The results, listed in Table 1, show the bulk composition of the outer region of pocket to be very similar to that of the host olivine, while the inner region (Figure 1c) exhibits a slightly higher Mg concentration (Table 1). We employed TEM to image a cross-section of the pocket (Figures 1d,e). Based on electron diffraction, the darkish grains can be identified as olivine crystals (Figure 1f,g) and the bright spherules as ferropericlase (Figure 1h). In agreement with SEM textural observations, the matrix in the inner region is mostly constituted of large olivine crystals. The presence of spherical ferropericlase in this region of the pocket is relatively scarce. Closer to the pocket wall, olivine grains within the matrix become smaller (100-500 nm in diameter) and the number of spherical ferropericlase crystals increases. Elemental maps of Si, Mg and Fe were collected in the outer region. The results clearly show an anti-correlation between Fe and Si resulting from Fe partitioning preferentially in the Si-free ferropericlase compared to olivine, and providing further evidence for the coexistence of ferropericlase and olivine within the investigated pocket (Figure 2). The Mg-map does not show any marked contrast because of the similar Mg content in ferropericlase and olivine.

The chemical compositions of various ferropericlase and olivine crystals from both regions of the pocket were determined with STEM-EDS analysis. Figures showing the location of the STEM-EDS analysis points (Figure S1, S2 and S3), as well as the results (Table S1, S2 and S3), are provided as supplementary material. STEM-EDS analysis results are plotted in the MgO-FeO-SiO_2 ternary diagram (Figure 3). According to our analysis, most of the olivine crystals constituting the matrix in the pocket are enriched in Mg with respect to the host olivine (Fa_{31}). The Mg enrichment is particularly highlighted in the results from the relatively large sized olivine crystals contained in the inner region of the pocket (Fa_{23}) (e.g., analysis point 002 and 009 in Table S2). We also observed the presence of olivine crystals with a composition very similar to that of the host olivine (e.g., analysis point 008 in Table S1), as well as a relatively Fe-rich olivine (Fa_{44}) in the inner region of the pocket (analysis points 019-021, Table S3). In addition, analyses on the matrix of the outer region highlighted the presence of Si concentrations higher than that stoichiometrically expected in olivine, but still lower than that of $(Mg,Fe)SiO_3$ (analysis point 007, Table S1). The presence of Si in the analysis on the nm-sized ferropericlase suggests that these analyses suffered from a contamination from the surrounding matrix since individual crystals smaller than the thickness of the TEM slice. To address this issue, ferropericlase compositions were corrected assuming that Si contained in the ferropericlase bulk analysis is due to a contamination of Mg-rich olivine, as the latter has been found to be the main constituent of the pocket matrix. Accordingly, an olivine with an assumed composition of Mg = 51, Fe = 15.7, Si = 33.3 (in mol%) was used for used for the correction of the ferropericlase composition. Olivine employed for the ferropericlase correction, as well as the corrected and original ferropericlase compositions are plotted in Figure 3. The FeO contents of ferropericlase corrected by subtraction of Mg-rich olivine in Figure 3 may be seen as an upper bound, since the matrix might contain quenched liquid composed of Fe-rich olivine and silica-rich interstitial amorphous materials resulting from the melting process.

Discussion

In natural shocked samples, ferropericlase has been thus far interpreted to form through solid state reactions (e.g., Miyahara et al., 2011, 2016), or as a product of melt crystallization (e.g., Chen et al., 1996). According to Miyahara et al. (2011), $(Mg,Fe)_2SiO_4$ olivine dissociation by solid state reaction displays characteristic textures: a lamellar texture of a $(Mg,Fe)SiO_3$ bridgmanite + (Mg,Fe)O ferropericlase tends to dominate the surrounding of the shock feature, evolving into a equigranular aggregate while approaching the interface with the host grain. The pocket studied here is entirely confined in an olivine grain, and none of the characteristic textures mentioned above are observed. In addition, experiments have shown that the dissociation of $(Mg,Fe)_2SiO_4$ polymorphs produces an assemblage which is dominated by a $(Mg,Fe)SiO_3$ phase, with (Mg,Fe)O ferropericlase occupying the remaining fraction (Liu 1979). In the basaltic shergottite DaG 735 for example, $(Mg,Fe)_2SiO_4$ olivine dissociated into an assemblage with a volume ratio between (Mg,Fe)O ferropericlase and $(Mg,Fe)SiO_3$ bridgmanite of about 30:70 (Miyahara et al. 2011). Our STEM-EDS analysis does not indicate the presence of $(Mg,Fe)SiO_3$ phase within the studied pocket. As noted above, areas showing higher Si concentrations than that stoichiometrically expected in olivine, but still lower than that of $(Mg,Fe)SiO_3$, were detected in the pocket (Figure 3). These Si-rich areas, however, appear to be too scarce to be associated with the presence of significant volumes of $(Mg,Fe)SiO_3$ phase as expected to be formed in the case of $(Mg,Fe)_2SiO_4$

olivine dissociation. All the above observations suggest that the lunar ferropericlase did not originate from the solid state reaction, hence its formation is likely linked to melting processes. Melting experiments have shown that Mg_2SiO_4 forsterite melts incongruently in a wide range of *P-T* conditions, encompassing pressures as low as 10-15 GPa at sufficiently high temperatures (> ~2200 °C), resulting in an assemblage of MgO periclase + liquid (Presnall and Walter, 1993). This incongruent melting occurs also in $(Mg,Fe)_2SiO_4$ olivine (Ohtani et al., 1998). Additionally, the chemical composition of ferropericlase formed by incongruent melting is very sensitive to temperature (Herzberg and Zhang 1996). Hence, if the incongruent melting of olivine occurred during the peak of shock compression but at different temperatures above the peritectic, it may result in ferropericlase covering a relatively wide compositional range, such as that observed in the lunar ferropericlase crystals studied here. Having considered this, as well as the absence of a $(Mg,Fe)SiO_3$ phase, we suggest that lunar ferropericlase has been formed primarily by shock induced incongruent melting of olivine. The incongruent melting of olivine can also well explain all the phases found to coexist within the studied pocket. In particular, Mg-rich olivine can be identified as the residual olivine from the melting process (Residual Ol in Figure 3), while the presence of Fe-rich olivine within pocket can be seen as a melt quenched product (Quenched Ol in Figure 3). A large spread in the Mg-Fe ratios in analysed ferropericlase is likely the result of different formation temperatures during shock metamorphism, that lead to the formation of Mg-rich ferropericlase during high temperatures and the subsequent enrichment in Fe while temperatures decreased during the quenching process (Herzberg and Zhang 1996). Ultimately, Si-rich areas detected in the matrix of the pocket can be seen as indicative of the presence of the residual liquid (Si-rich in Figure 3), which is also expected to be a product of the incongruent melting. On the other hand, the presence of olivine crystals with a composition similar to that of the host olivine may suggest the presence of recrystallized host olivine that did not undergo melting during shock metamorphism, although we cannot exclude them to be fragments of the host olivine that simply did not experience incongruent melting (Recrystalized/Fragmented Ol in Figure 3). Another possible scenario may see ferropericlase crystalizing from a melt at temperatures exceeding the liquidus, and subsequently followed by the crystallization of olivine at the peritectic temperature. If this was the case, however, we would expect ferropericlase to have a relatively homogeneous chemical composition given by the rapid thermal equilibration of the melt as was reported by Chen et al. (1996). On the contrary, the ferropericlase crystals observed in this study cover a wide range of composition - an observation that is difficult to reconcile with the scenario involving melt crystallization as a primary process for the ferropericlase formation.

In ordinary chondrites, wadsleyite and ringwoodite aggregates have been typically found within and/or in the surrounding of the shock features (Chen et al. 2004; Yin et al. 2018; Miyahara et al. 2020), and ringwoodite has been also found in association with ferropericlase (Chen et al. 1996). It has been proposed that the combination of relatively high temperature and low pressures that characterize retrograde events leads to the back-transformation of ringwoodite into wadsleyite (Madon and Poirier 1983; Price et al. 1983), or even into olivine, as for example reported for the Mbale and Y-75267 ordinary chondrites (Chen et al. 1998; Kimura et al. 2004; Hu and Sharp 2017; Fukimoto et al. 2020). In order for reverse transformations to occur, however, the shock feature needs to be quenched at relatively slow rates, maintaining high temperatures for a few seconds (Kimura et al. 2004; Ohtani et al. 2004). A relatively rapid quench of the shock feature hampers back-transformation reactions, leading to the preservation of the high-pressure polymorphs. The thickness of the studied pocket is about 10 μm. We therefore expect an effective thermal equilibration with the host olivine during the retrograde path of the shock event, resulting in a rapid

This is the peer-reviewed, final accepted version for American Mineralogist, published by the Mineralogical Society of America.
The published version is subject to change. Cite as Authors (Year) Title. American Mineralogist, in press.
DOI: https://doi.org/10.2138/am-2022-8121. http://www.minsocam.org/

quench of the pocket. Following the approach delineated by Langenhorst and Poirier (2000), we estimated the solidification of the pocket to occur within microseconds (see Text S1). We did not find any evidence for the presence of any of the $(Mg,Fe)_2SiO_4$ high-pressure polymorphs in our sample. Despite the possibility that wadsleyite formation may have been inhibited by the relatively high Fe concentration in the host olivine (Fa_{31}) (Frost 2003; Tsujino et al. 2019), the absence of ringwoodite suggests that *P-T* conditions necessary for its formation were not reached to during the shock event, since it would otherwise have been preserved given the rapid quenching process. If (Mg,Fe)O ferropericlase formed as a result of the incongruent melting of olivine induced by a shock event, as suggested by our observations, we estimate the *P-T*-conditions reached during the impact event to fall in the range of 12-17 GPa and 2250-2450 °C based on the results of previous experimental works on the phase relations in the Mg_2SiO_4 system (Presnall and Walter 1993) (Figure 4). However, according to melting experiments in the $(Mg,Fe)_2SiO_4$ system, the addition of a fayalitic component to the Mg_2SiO_4 system would shift the incongruent melting towards lower temperatures (Ohtani et al., 1998). Additionally, the absence of ringwoodite suggests that shock pressures at the peak conditions likely did not exceed 15 GPa (Frost 2003; Tsujino et al. 2019). Hence, we expect the comparison with static high-pressure experiments in the Mg_2SiO_4 system to serve as the upper bound for the estimate of the shock *P-T* condition.

It is important however to consider that an excess of pressure and temperature is commonly required to trigger nucleation and growth of high-pressure phases, bringing additional uncertainties in the shock-induced *P-T* conditions when those are estimated by linking a given suite of high-pressure minerals to phase relations derived by static compression experiments (Sharp and De Carli 2006). However, according to our interpretation, the ferropericlase formation process discussed here occurred at relatively high temperatures, hence in an environment characterized by relatively rapid nucleation and growth rates. Therefore, we expect that incongruent melting boundaries derived by static high-pressure experiments can be used to confidently estimate the *P*-*T* conditions reached during the shock event recorded the studied section. We also acknowledge that recent advances in dynamic compression experiments could allow the investigation of the effects that nucleation and growth kinetics have on the phase boundaries (Jenei et al. 2019; Méndez et al. 2020), thus providing a tool to better interpret high-pressure mineralogy in shocked materials (e.g., Carl et al. 2017, 2018; Černok et al. 2017; Sims et al. 2019; Husband et al. 2021).

Despite suggesting the incongruent melting of olivine to be the primary process of ferropericlase formation, we cannot exclude that some of the ferropericlase crystals observed (particularly those exhibiting relatively high Mg concentrations) might have crystallized from a melt that formed as a result of temperature exceeding the liquidus locally during shock metamorphism.

In general, the estimated shock pressure conditions are in good agreement with the finding of SiO_2 stishovite in the Apollo Sample 15299 by Kaneko et al. (2015). Since the shock pressure is generally proportional to the impact velocity in dynamic events (Melosh 1989), our observations suggest that the shock features recorded in S247 are either the result of a low velocity impact, or that the Apollo Sample 15299 was only exposed to attenuated shock pressure due to a relatively distant location from the centre of the impact.

Implications

Across the first few kilometres depth, the Moon's surface is characterized by a layer of unconsolidated and porous materials, including lithic and mineral fragments shattered by countless impact events (Huang and Wieczorek 2012). Lunar rocks lithified by shock compression (Kieffer and Simonds 1980; Huang and Wieczorek 2012), i.e. regolith breccia, are characterized by shock-related microfractures causing pervasive porosities up to 15-22% (Kiefer et al. 2012), which are typically higher than those reported in most meteorites (Warren 2001; Consolmagno et al. 2008). Porosity has a strong effect on the response of a material to shock compression since the first stage of shock compression of a porous material is characterized by a collapse of the void. The void collapse process can produce an increase in thermal energy that translates into relatively high temperature even at low pressure conditions (Sharp and De Carli 2006; Hirata et al. 2009; Meyer et al. 2011; Levesque and Vitello 2015). Additionally, the textural complexity of a porous material can lead to a heterogeneous temperature distribution during shock compression, resulting in localized spikes in the *P*-*T* conditions experienced by the material during the shock event (Kieffer 1971; Hirata et al. 2009). Our observations suggest that the olivine grain contained in the basalt clast of S247 was likely characterized by a pre-existing system of fracture that collapsed as a result of shock compression. The fracture collapse could induce localized spikes in the shock temperatures, resulting in the incongruent melting of olivine from which lunar ferropericlase originated.

Acknowledgements

We are grateful to the NASA's Johnson Space Center for providing us a chance to study the Apollo section 15299,247 with T. Arai as a primary investigator. We appreciate T. Miyazaki of Tohoku University for his assistance with TEM analysis. N. Satta thanks T. Boffa Ballaran and N. Miyajima of BGI for the helpful discussions. The authors thanks Steve Simon, Makoto Kimura and another anonymous reviewer for their comments. N. Satta was supported by the International Research Training Group "Deep Earth Volatile Cycles" (GRK 2156/1), the European Union's Horizon 2020 research and innovation Programme (ERC grant 864877), as well as the JSPS

This is the peer-reviewed, final accepted version for American Mineralogist, published by the Mineralogical Society of America.
The published version is subject to change. Cite as Authors (Year) Title. American Mineralogist, in press.
DOI: https://doi.org/10.2138/am-2022-8121. http://www.minsocam.org/

Japanese-German graduate externship for Research on Deep Earth Volatile Cycle and the International Joint Graduate Program in Earth and Environmental Sciences (GP-EES) of Tohoku University. E. Ohtani was supported by Kakenhi Grant Number JP15H05748 and JP20H00187, and by the research award from the Alexander von Humboldt foundation. An early draft of this manuscript was included in Satta (2021).

Contributions

E. Ohtani, N.Satta and H. Marquardt conceived this study. T. Arai and E. Ohtani selected the sample. N. Satta, M. Mayahara, S. Ozawa, and E. Ohtani were involved in the collection, analysis and interpretation of the data. M. Nishijima operated the focused ion beam. N.Satta, E. Ohtani, M. Miyahara and H. Marquardt wrote the manuscript.

References

Bindi, L., Shim, S.-H., Sharp, T.G., and Xie, X. (2020) Evidence for the charge disproportionation of iron in extraterrestrial bridgmanite. Science Advances, 6, eaay7893.

Carl, E.-R., Mansfeld, U., Liermann, H.-P., Danilewsky, A., Langenhorst, F., Ehm, L., Trullenque, G., and Kenkmann, T. (2017) High-pressure phase transitions of α-quartz under nonhydrostatic dynamic conditions: A reconnaissance study at PETRA III. Meteoritics & Planetary Science, 52, 1465–1474.

Carl, E.-R., Liermann, H.-P., Ehm, L., Danilewsky, A., and Kenkmann, T. (2018) Phase transitions of α-quartz at elevated temperatures under dynamic compression using a membrane-driven diamond anvil cell: Clues to impact cratering? Meteoritics & Planetary Science, 53, 1687–1695.

Černok, A., Marquardt, K., Caracas, R., Bykova, E., Habler, G., Liermann, H.-P., Hanfland, M., Mezouar, M., Bobocioiu, E., and Dubrovinsky, L. (2017) Compressional pathways of α-cristobalite, structure of cristobalite X-I, and towards the understanding of seifertite formation. Nature Communications, 8, 15647.

Chen, M., Sharp, T.G., El Goresy, A., Wopenka, B., and Xie, X. (1996) The Majorite-Pyrope + Magnesiowüstite Assemblage: Constraints on the History of Shock Veins in Chondrites. Science, 271, 1570–1573.

Chen, M., Xie, X., El Goresy, A., Wopenka, B., and Sharp, T.G. (1998) Cooling rates in the shock veins of chondrites: constraints on the (Mg, Fe) 2 SiO 4 polymorph transformations. Science in China Series D: Earth Sciences, 41, 522–528.

Chen, M., El Goresy, A., and Gillet, P. (2004) Ringwoodite lamellae in olivine: Clues to olivine–ringwoodite phase transition mechanisms in shocked meteorites and subducting slabs. Proceedings of the National Academy of Sciences, 101, 15033–15037.

Consolmagno, G.J., Britt, D.T., and Macke, R.J. (2008) The significance of meteorite density and porosity. Geochemistry, 68, 1–29.

Frost, D.J. (2003) The structure and sharpness of (Mg,Fe)2SiO4 phase transformations in the transition zone. Earth and Planetary Science Letters, 216, 313–328.

——— (2008) The upper mantle and transition zone. Elements, 4, 171–176.

Fukimoto, K., Miyahara, M., Sakai, T., Ohfuji, H., Tomioka, N., Kodama, Y., Ohtani, E., and Yamaguchi, A. (2020) Back-transformation mechanisms of ringwoodite and majorite in an ordinary chondrite. Meteoritics & Planetary Science, 55.

Gillet, P., and El Goresy, A. (2013) Shock Events in the Solar System: The Message from Minerals in Terrestrial Planets and Asteroids. Annual Review of Earth and Planetary Sciences, 41, 257–285.

Gillet, P., El Goresy, A., Beck, P., and Chen, M. (2007) High-pressure mineral assemblages in shocked meteorites and shocked terrestrial rocks: Mechanisms of phase transformations and constraints to pressure and temperature histories. In Advances in High-Pressure Mineralogy. Geological Society of America.

Herzberg, C., and Zhang, J. (1996) Melting experiments on anhydrous peridotite KLB-1: Compositions of magmas in the upper mantle and transition zone. Journal of Geophysical Research: Solid Earth, 101, 8271–8295.

Hirata, N., Kurita, K., and Sekine, T. (2009) Simulation experiments for shocked primitive materials in the Solar System. Physics of the Earth and Planetary Interiors, 174, 227–241.

Hu, J., and Sharp, T.G. (2017) Back-transformation of high-pressure minerals in shocked chondrites: Low-pressure mineral evidence for strong shock. Geochimica et Cosmochimica Acta, 215, 277–294.

Huang, Q., and Wieczorek, M.A. (2012) Density and porosity of the lunar crust from gravity and topography. Journal of Geophysical Research: Planets, 117.

Husband, R.J., O'Bannon, E.F., Liermann, H.-P., Lipp, M.J., Méndez, A.S.J., Konôpková, Z., McBride, E.E., Evans, W.J., and Jenei, Z. (2021) Compression-rate dependence of pressure-induced phase transitions in Bi. Scientific Reports, 11, 14859.

Ito, E., and Takahashi, E. (1989) Postspinel transformations in the system Mg2SiO4-Fe2SiO4 and some geophysical implications. Journal of Geophysical Research: Solid Earth, 94, 10637–10646.

Jenei, Zs., Liermann, H.P., Husband, R., Méndez, A.S.J., Pennicard, D., Marquardt, H., O'Bannon, E.F., Pakhomova, A., Konopkova, Z., Glazyrin, K., and others (2019) New dynamic diamond anvil cells for tera-pascal per second fast compression x-ray diffraction experiments. Review of Scientific Instruments, 90, 065114.

Kaneko, S., Miyahara, M., Ohtani, E., Arai, T., Hirao, N., and Sato, K. (2015) Discovery of stishovite in Apollo 15299 sample. American Mineralogist, 100, 1308–1311.

Kayama, M., Tomioka, N., Ohtani, E., Seto, Y., Nagaoka, H., Götze, J., Miyake, A., Ozawa, S., Sekine, T., Miyahara, M., and others (2018) Discovery of moganite in a lunar meteorite as a trace of H2O ice in the Moon's regolith. Science Advances, 4, eaar4378.

Kiefer, W.S., Macke, R.J., Britt, D.T., Irving, A.J., and Consolmagno, G.J. (2012) The density and porosity of lunar rocks: THE DENSITY AND POROSITY OF LUNAR ROCKS. Geophysical Research Letters, 39, n/a-n/a.

Kieffer, S.W. (1971) Shock metamorphism of the Coconino Sandstone at Meteor Crater, Arizona. Journal of Geophysical Research (1896-1977), 76, 5449–5473.

Kieffer, S.W., and Simonds, C.H. (1980) The role of volatiles and lithology in the impact cratering process. Reviews of Geophysics, 18, 143–181.

Kimura, M., Chen, M., Yoshida, Y., El Goresy, A., and Ohtani, E. (2004) Back-transformation of high-pressure phases in a shock melt vein of an H-chondrite during atmospheric passage: Implications for the survival of high-pressure phases after decompression. Earth and Planetary Science Letters, 217, 141–150.

Langenhorst, F., and Hornemann, U. (2005) Shock experiments on minerals: Basic physics and techniques. In G. Papp, T.G. Weiszburg, and R. Miletich, Eds., Mineral behaviour at extreme conditions pp. 357–387. Mineralogical society of Great Britain and Ireland, London.

Langenhorst, F., and Poirier, J.-P. (2000) Anatomy of black veins in Zagami: clues to the formation of high-pressure phases. Earth and Planetary Science Letters, 184, 37–55.

Levesque, G.A., and Vitello, P. (2015) The Effect of Pore Morphology on Hot Spot Temperature. Propellants, Explosives, Pyrotechnics, 40, 303–308.

Liu, L.-G. (1979) Calculations of high-pressure phase transitions in the system $MgO-SiO_2$ and implications for mantle discontinuities. Physics of the Earth and Planetary Interiors, 19, 319–330.

Madon, M., and Poirier, J.P. (1983) Transmission electron microscope observation of α, β and γ $(Mg, Fe)_2SiO_4$ in shocked meteorites: planar defects and polymorphic transitions. Physics of the Earth and Planetary Interiors, 33, 31–44.

Melosh, H.J. (1989) Impact Cratering: A Geologic Process, 256 p. New York: Oxford University Press.

Méndez, A.S.J., Marquardt, H., Husband, R.J., Schwark, I., Mainberger, J., Glazyrin, K., Kurnosov, A., Otzen, C., Satta, N., Bednarcik, J., and others (2020) A resistively-heated dynamic diamond anvil cell (RHdDAC) for fast compression x-ray diffraction experiments at high temperatures. Review of Scientific Instruments, 91, 073906.

Meyer, C., Fritz, J., Misgaiski, M., Stöffler, D., Artemieva, N.A., Hornemann, U., Moeller, R., Vera, J.-P.D., Cockell, C., Horneck, G., and others (2011) Shock experiments in support of the Lithopanspermia theory: The influence of host rock composition, temperature, and shock pressure on the survival rate of endolithic and epilithic microorganisms. Meteoritics & Planetary Science, 46, 701–718.

Miyahara, M., Ohtani, E., Ozawa, S., Kimura, M., El Goresy, A., Sakai, T., Nagase, T., Hiraga, K., Hirao, N., and Ohishi, Y. (2011) Natural dissociation of olivine to $(Mg,Fe)SiO_3$ perovskite and magnesiowüstite in a shocked Martian meteorite. Proceedings of the National Academy of Sciences, 108, 5999–6003.

Miyahara, M., Kaneko, S., Ohtani, E., Sakai, T., Nagase, T., Kayama, M., Nishido, H., and Hirao, N. (2013) Discovery of seifertite in a shocked lunar meteorite. Nature Communications, 4, 1737.

Miyahara, M., Ohtani, E., El Goresy, A., Ozawa, S., and Gillet, P. (2016) Phase transition processes of olivine in the shocked Martian meteorite Tissint: Clues to origin of ringwoodite-, bridgmanite- and magnesiowüstite-bearing assemblages. Physics of the Earth and Planetary Interiors, 259, 18–28.

Miyahara, M., Yamaguchi, A., Saitoh, M., Fukimoto, K., Sakai, T., Ohfuji, H., Tomioka, N., Kodama, Y., and Ohtani, E. (2020) Systematic investigations of high-pressure polymorphs in shocked ordinary chondrites. Meteoritics & Planetary Science, 55, 2619–2651.

Morbidelli, A., Lunine, J.I., O'Brien, D.P., Raymond, S.N., and Walsh, K.J. (2012) Building Terrestrial Planets. Annual Review of Earth and Planetary Sciences, 40, 251–275.

DOI: https://doi.org/10.2138/am-2022-8121. http://www.minsocam.org/

Ohtani, E., Moriwaki, K., Kato, T., and Onuma, K. (1998) Melting and crystal–liquid partitioning in the system Mg2SiO4–Fe2SiO4 to 25 GPa. Physics of the Earth and Planetary Interiors, 107, 75–82.

Ohtani, E., Kimura, Y., Kimura, M., Takata, T., Kondo, T., and Kubo, T. (2004) Formation of high-pressure minerals in shocked L6 chondrite Yamato 791384: constraints on shock conditions and parent body size. Earth and Planetary Science Letters, 227, 505–515.

Ohtani, E., Ozawa, S., Miyahara, M., Ito, Y., Mikouchi, T., Kimura, M., Arai, T., Sato, K., and Hiraga, K. (2011) Coesite and stishovite in a shocked lunar meteorite, Asuka-881757, and impact events in lunar surface. Proceedings of the National Academy of Sciences, 108, 463–466.

Presnall, D.C., and Walter, M.J. (1993) Melting of forsterite, Mg2SiO4, from 9.7 to 16.5 GPa. Journal of Geophysical Research: Solid Earth, 98, 19777–19783.

Price, G.D., Putnis, A., Agrell, S.O., and Smith, D.G.W. (1983) Wadsleyite, natural beta -(Mg, Fe) 2 SiO 4 from the Peace River Meteorite. The Canadian Mineralogist, 21, 29–35.

Satta, N. (2021) High Pressure Minerals in the Earth and Moon: Understanding the Lunar Impact History and Earth's Deep Water Cycle. Doctoral thesis, Bayreuth.

Schmitt, D.R., and Ahrens, T.J. (1983) Temperatures of shock-induced shear instabilities and their relationship to fusion curves. Geophysical Research Letters, 10, 1077–1080.

Sharp, T.G., and De Carli, P.S. (2006) Shock Effects in Meteorites. In Meteorites and the Early Solar System II pp. 653–677.

Simon, S.B., Papike, J.J., Gosselin, D.C., and Laul, J.C. (1986) Petrology, chemistry and origin of Apollo 15 regolith breccias. Geochimica et Cosmochimica Acta, 50, 2675–2691.

Sims, M., Jaret, S.J., Carl, E.-R., Rhymer, B., Schrodt, N., Mohrholz, V., Smith, J., Konopkova, Z., Liermann, H.-P., Glotch, T.D., and others (2019) Pressure-induced amorphization in plagioclase feldspars: A time-resolved powder diffraction study during rapid compression. Earth and Planetary Science Letters, 507, 166–174.

Swann, G.A., Bailey, N.G., Batson, R.M., Freeman, V.L., Hait, M.H., Head, J.W., Holt, H.E., Howard, K.A., Irwin, J.B., Larson, K.B., and others (1972) Preliminary geologic investigation of the Apollo 15 landing site. In Apollo 15 Preliminary Science Report Vol. 5–1. National Aeronautics and Space Administration.

Tschauner, O., Ma, C., Beckett, J.R., Prescher, C., Prakapenka, V.B., and Rossman, G.R. (2014) Discovery of bridgmanite, the most abundant mineral in Earth, in a shocked meteorite. Science, 346, 1100–1102.

Tsujino, N., Yoshino, T., Yamazaki, D., Sakurai, M., Sun, W., Xu, F., Tange, Y., and Higo, Y. (2019) Phase transition of wadsleyite-ringwoodite in the Mg2SiO4-Fe2SiO4 system. American Mineralogist, 104, 588–594.

Warren, P.H. (2001) Porosities of lunar meteorites: Strength, porosity, and petrologic screening during the meteorite delivery process. Journal of Geophysical Research: Planets, 106, 10101–10111.

Yin, F., Liao, Z., Hursthouse, A., and Dai, D. (2018) Shock-Induced Olivine-Ringwoodite Transformation in the Shock Vein of Chondrite GRV053584. Minerals, 8, 139.

Table 1. Results of SEM-EDS analyses on the host olivine and pocket in S247**.**

	Host olivine	**Pocket inner region**	**Pocket outer region**
Oxides			
SiO_2	37.5(2)	37.6(1)	37.6(2)
Al_2O_3	0.06(5)	0.2(1)	0.3(1)
FeO	27.9(2)	26(1)	27.8(9)
MgO	34.3(3)	35.8(1)	33.8(9)
CaO	0.2(1)	0.5(1)	0.6(1)
Total (wt%)	100	100	100
APFU			
Si	1.00(1)	0.99(1)	1.01(1)
Al	0.0	0.1	0
Fe	0.62(1)	0.58(2)	0.62(2)
Mg	1.37(1)	1.41(1)	1.35(4)
Ca	0.1	0.1	0.2
n	6	5	6

Analyses are normalized to 100%. All Fe is assumed ferrous. Numbers in parenthesis are standard deviations in the last reported digit. APFU are calculated assuming O=4. n = sample size.

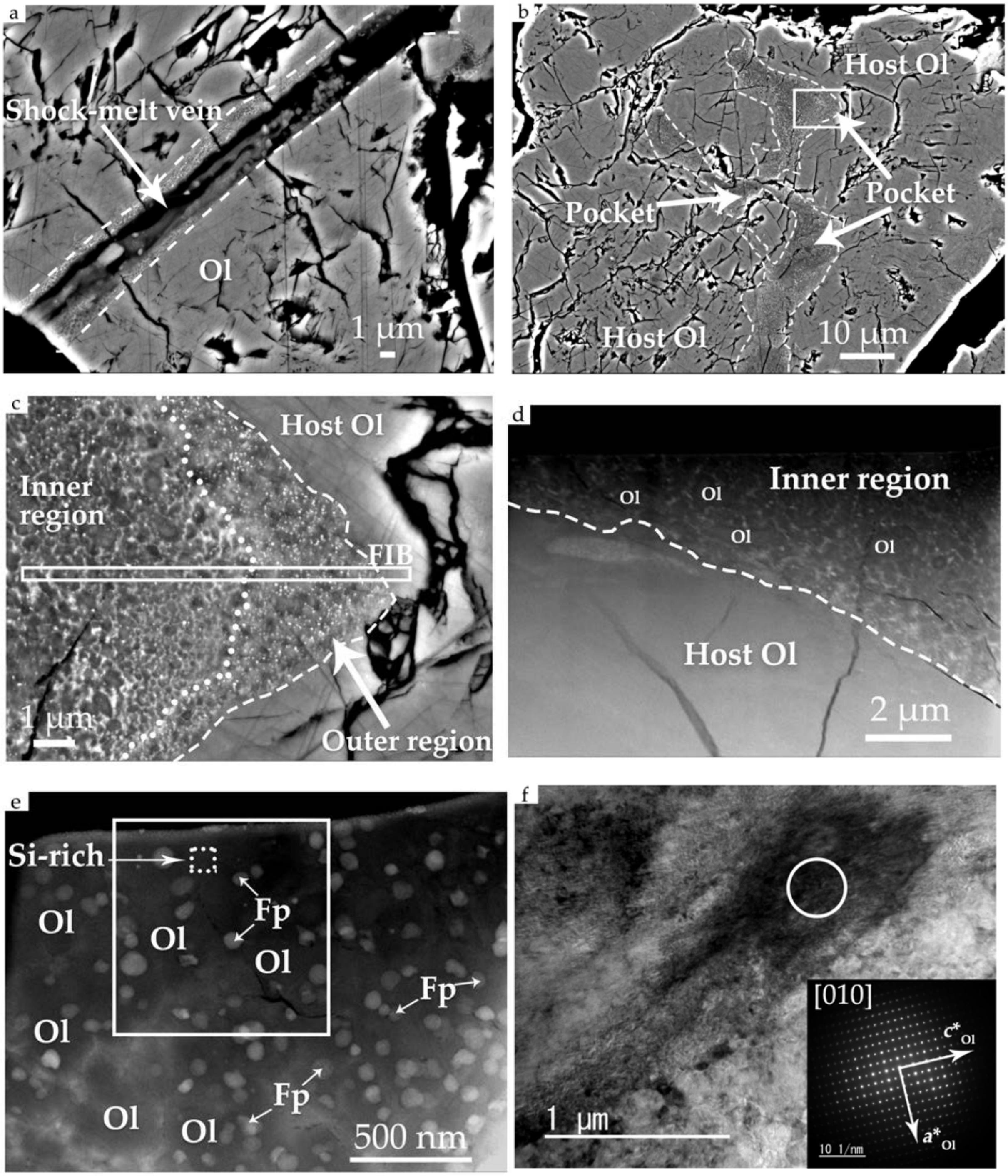
a
Shock-melt vein
Ol
1 μm
b
Host Ol
Pocket
Pocket
Host Ol
10 μm
c
Host Ol
Inner region
FIB
1 μm
Outer region
d
Inner region
Ol
Ol
Ol
Ol
Host Ol
2 μm
e
Si-rich
Fp
Ol
Ol
Ol
Ol
Fp
Ol
Ol
Fp
500 nm
f
[010]
c*Ol
a*Ol
10 1/nm
1 μm

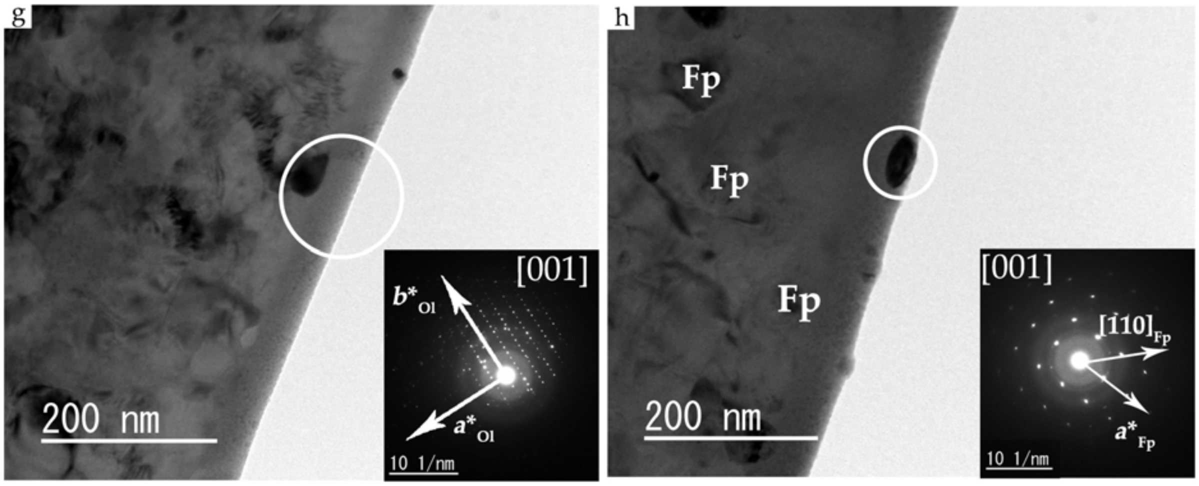

Figure 1. Scanning Electron Microscopy (SEM) and Transmission Electron Microscopy (TEM) images of the investigated shock-melt pocket. a) Back-scattered Electron (BSE) image collected with a field emission gun SEM of a shock-melt vein contained in the studied section; b) BSE image of the investigated shock-melt pocket. White square shows the location of Fig.1c; c) High magnification BSE image of the of the shock-melt pocket. White box shows the location of the block extracted using FIB; d) and e) High-Angle Annular Dark Field (HAADF) images exposing in the inner and outer regions of shock-melt pocket, respectively. White solid box shows the area of the elemental mapping, dashed box denotes the location of the chemical analysis point in which a Si-rich area was identified. Ol = olivine, Fp = ferropericlase f) and g) Bright-field (BF)-TEM images of olivine grains contained in the inner and outer regions, respectively. White circles show the locations of the investigate crystals. SAED patterns are shown as inset figures. h) BF-TEM image of ferropericlase crystals. Inset box shows the SAED pattern of the ferropericlase crystal within the white circle.

DOI: https://doi.org/10.2138/am-2022-8121. http://www.minsocam.org/

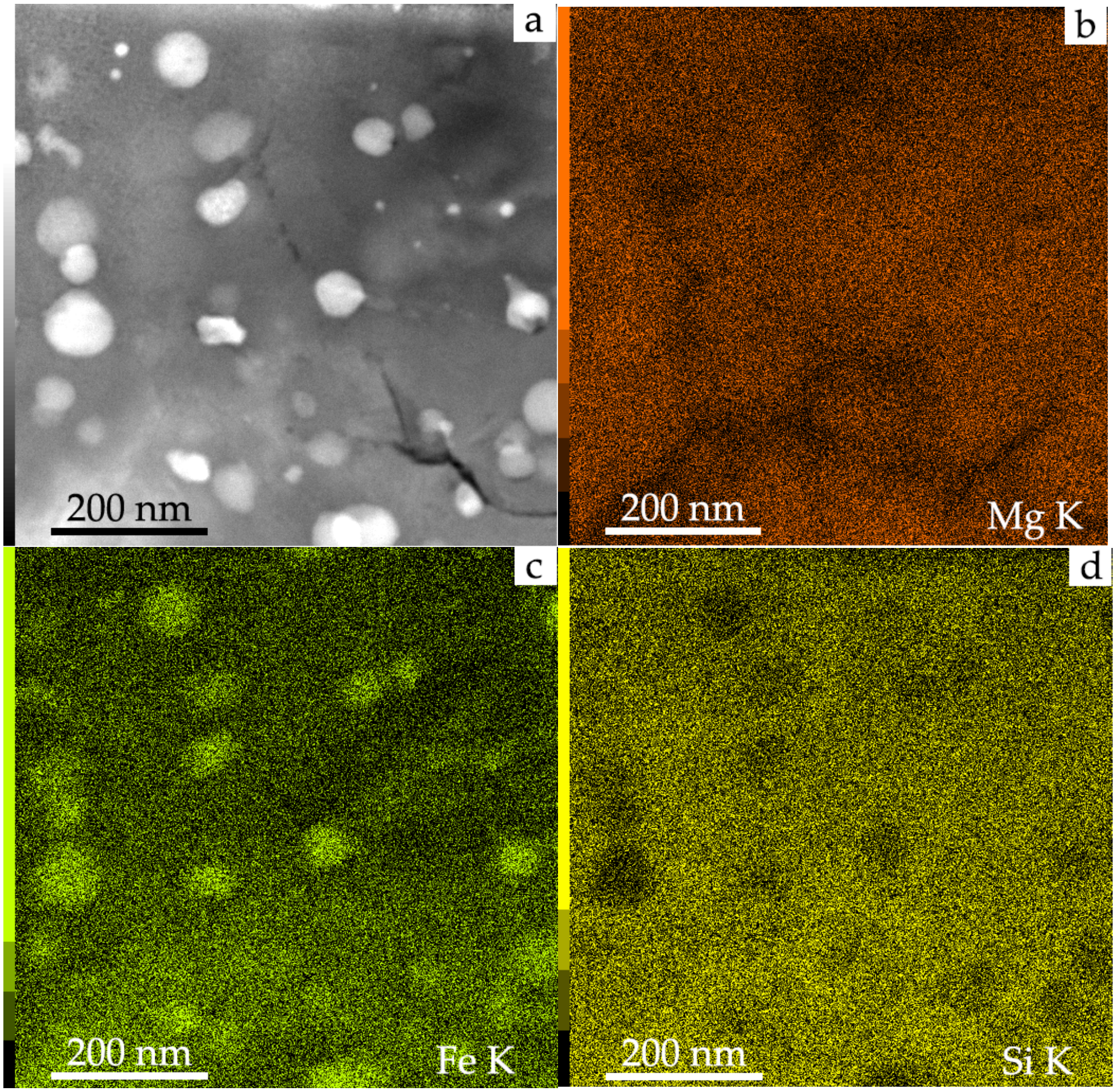

Figure 2. High-Angle Annular Dark-Field **(**HAADF) image and elemental mapping of the outer region of the shock melt pocket. (a) HAADF image; (b-d) elemental mapping images obtained with STEM-EDS showing the coexistence of ferropericlase + olivine crystals. Granular crystals are ferropericlase and the matrix part is mainly composed of olivine.

DOI: https://doi.org/10.2138/am-2022-8121. http://www.minsocam.org/

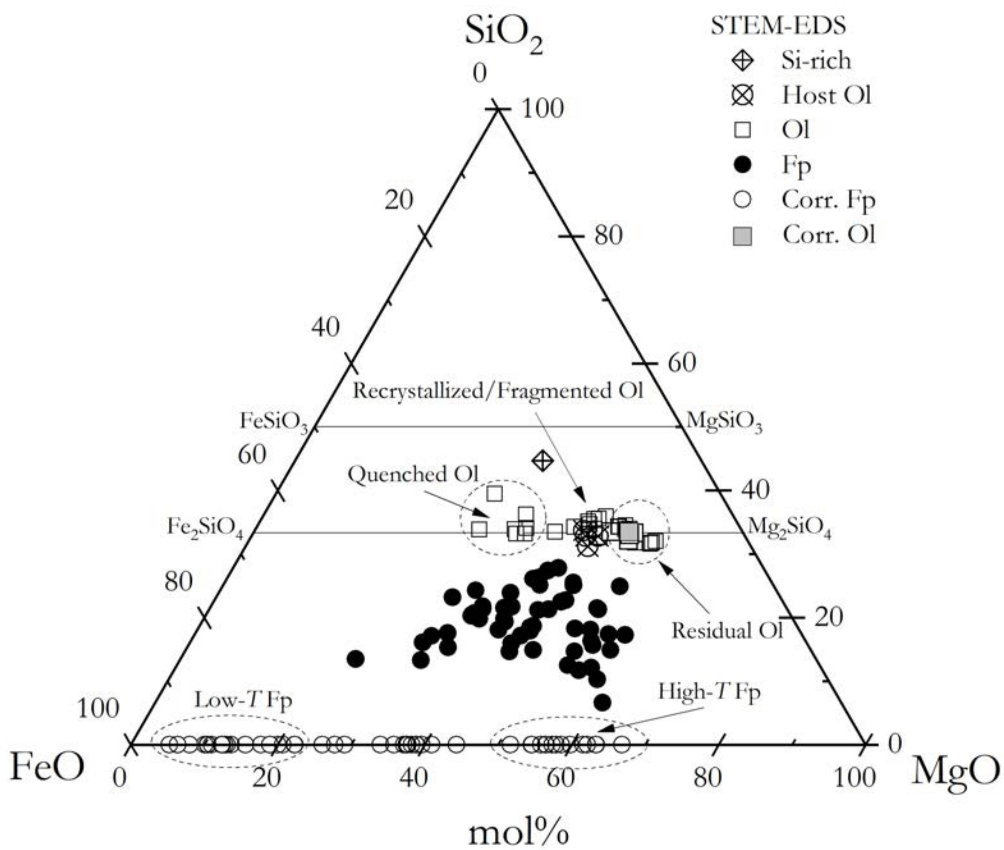

Figure 3. The results of the STEM-EDS analysis of ferropericlase and olivine in the shock melt pocket plotted in a MgO-FeO-SiO_2 diagram. The contaminated compositions of ferropericlase were corrected by subtraction of the matrix olivine and shown as open circles. Grey square shows the composition of the olivine used for the correction of ferropericlase composition. A measured point shown as “Si-rich” may suggest the presence of a silicate residual liquid. Fp = ferropericlase, Corr. Fp = corrected ferropericlase, Corr. Ol = olivine used for the correction of ferropericlase composition, Ol = olivine.

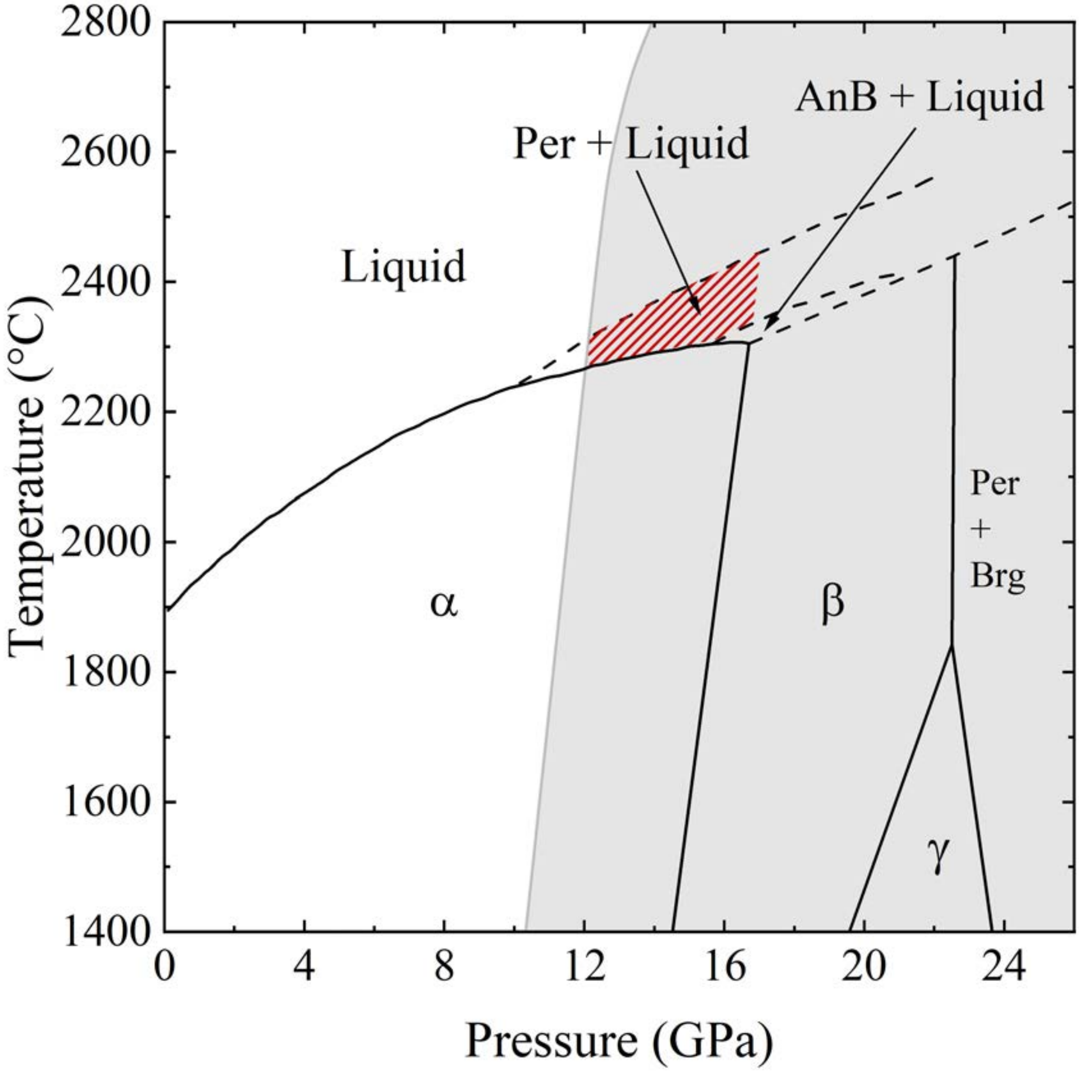

Figure 4. P-T conditions estimated from the high-pressure assemblages contained in the shock melt pocket of the studied section are shown as are shown as shaded region in red. Phase relations in the Mg_2SiO_4 system are from (Presnall and Walter 1993). Light grey shaded area shows the P-T stability field of SiO_2 stishovite (Schmitt and Ahrens 1983). Per = periclase, Brg = bridgmanite, α = olivine, β = wadsleyite, γ = ringwoodite and AnB = anhydrous phase B.